Journal of Materials Chemistry A

PAPER

View Article Online
View Journal | View Issue

Cite this: J. Mater. Chem. A, 2014, 2, 7780

A CO_2-stable reduction-tolerant Nd-containing dual phase membrane for oxyfuel CO_2 capture†

Huixia Luo,*[ab] Tobias Klande,[a] Zhengwen Cao,[a] Fangyi Liang,[a] Haihui Wang*[c] and Jürgen Caro*[a]

Received 25th November 2013
Accepted 9th March 2014

DOI: 10.1039/c3ta14870j

www.rsc.org/MaterialsA

We report a novel CO_2-stable reduction-tolerant dual-phase oxygen transport membrane 40 wt% $Nd_{0.6}Sr_{0.4}FeO_{3-\delta}$–60 wt% $Ce_{0.9}Nd_{0.1}O_{2-\delta}$ (40NSFO–60CNO), which was successfully developed by a facile one-pot EDTA–citric sol–gel method. The microstructure of the crystalline 40NSFO–60CNO phase was investigated by combined *in situ* X-ray diffraction (XRD), scanning electron microscopy (SEM), back scattered SEM (BSEM), and energy dispersive X-ray spectroscopy (EDXS) analyses. Oxygen permeation and long-time stability under CO_2 and CH_4 atmospheres were investigated. A stable oxygen flux of 0.21 $cm^3\ min^{-1}\ cm^{-2}$ at 950 °C with undiluted CO_2 as sweep gas is found which is increased to 0.48 $cm^3\ min^{-1}\ cm^{-2}$ if the air side is coated with a porous $La_{0.6}Sr_{0.4}CoO_{3-\delta}$ (LSC) layer. All the experimental results demonstrate that the 40NSFO–60CNO not only shows good reversibility of the oxygen permeation fluxes upon temperature cycling, but also good phase stability in a CO_2 atmosphere and under the harsh conditions of partial oxidation of methane to synthesis gas up to 950 °C.

Introduction

Mixed ionic-electronic conducting oxygen transport materials (OTMs) offer high potential applications as a cathode in solid oxide fuel cells (SOFCs),[1,2] as a membrane or an adsorbent for oxygen production from air or other oxygen containing gases, or in membrane reactors for partial hydrocarbon oxidation.[3–6] A challenging application of OTMs would be the oxyfuel process with integrated CO_2 capture.[7,8] However, to survive under real process conditions in the presence of harsh gases (such as CO_2, H_2, CH_4, *etc.*) at high temperatures, a dense oxygen separation membrane should possess the following properties: (i) high oxygen permeation fluxes; (ii) good structural stability within appropriate ranges of temperature and oxygen partial pressure; (iii) sufficient chemical compatibility and mechanical strength.[9]

The state-of-the-art OTMs are mostly oxygen deficient perovskites containing Ba and/or Sr on the A-site and Co/Fe on the B-site since these cations match the perovskite lattice (Goldschmidt's tolerance factor[10]), but also because of their low manufacturing cost, simple design and high oxygen ion transport rates.[11–13] Even though these perovskite-type OTMs show high oxygen permeation fluxes, their poor thermo-mechanical strength, their low chemical stability, and their unsatisfied long-term stability under CO_2/SO_2 atmospheres or at low oxygen partial pressures are still the major barriers for widespread applications.[14–16] Especially, most of the single phase perovskite-type OTMs contain high basicity alkaline-earth ions, and are, therefore, susceptible to carbonate formation in a CO_2 containing atmosphere.[17–19]

Recently, some dual phase composite membranes, which consist of an oxygen ionic conducting (OIC) phase and an electronic conducting (EC) phase in a micro-scale phase mixture, have been developed and exhibit high steady oxygen permeation in CO_2 atmospheres, such as $NiFe_2O_4$–$Ce_{0.9}Gd_{0.1}O_{2-\delta}$,[7,20] Fe_2O_3–$Ce_{0.9}Gd_{0.1}O_{2-\delta}$,[21] $Mn_{1.5}Co_{1.5}O_{4-\delta}$–$Ce_{0.9}Pr_{0.1}O_{2-\delta}$,[22] $SmMn_{1.5}Co_{1.5}O_{4-\delta}$–$Ce_{0.9}Sm_{0.1}O_{2-\delta}$,[23] $Ba_{0.5}Sr_{0.5}Fe_{0.2}Co_{0.8}O_{3-\delta}$–$Ce_{0.9}Gd_{0.1}O_{2-\delta}$,[24] $La_{0.9}Sr_{0.1}FeO_{3-\delta}$–$Ce_{0.9}Sm_{0.1}O_{2-\delta}$, *etc.*[25] However, some problems still exist; for instance, (a) the ease to reduce Co and/or Ni metal ions in the EC phase with a large dependence of the ionic radius on the valence state which is unfavorable for membrane stability under a large oxygen concentration gradient;[7,20–23] (b) chemical compatibility and stability of the two phases by blocked cation diffusion between the two phases.[25]

It is known that the oxygen permeation and stability properties of the dual phase membrane depend strongly on their electronic and ionic conductivity, on the chemical compatibility, and phase and chemical stability. Therefore, based on our previous studies on dual phase membranes,[20–22] here we design a novel cobalt-free noble-metal free CO_2-stable and

[a]Institute of Physical Chemistry and Electrochemistry, Leibniz University of Hannover, Callinstr. 3A, D-30167, Hannover, Germany. E-mail: juergen.caro@pci.uni-hannover.de; Fax: +49 511 762 19121; Tel: +49 511 762 3175

[b]Department of Chemistry, Princeton University, Princeton, New Jersey 08544, USA. E-mail: huixial@princeton.edu; Fax: +1 609 258 6746; Tel: +1 609 258 5556

[c]School of Chemistry & Chemical Engineering, South China University of Technology, No. 381 Wushan Road, 510640 Guangzhou, China. E-mail: hhwang@scut.edu.cn; Fax: +86 020 8711 0131; Tel: +86 020 8711 0131

† Electronic supplementary information (ESI) available. See DOI: 10.1039/c3ta14870j

reduction-tolerant dual phase membrane material, 40 wt% $Nd_{0.6}Sr_{0.4}FeO_{3-\delta}$–60 wt% $Ce_{0.9}Nd_{0.1}O_{2-\delta}$ (abbreviated as 40NSFO–60CNO). In this dual phase system, CNO is the main OIC phase, and NSFO is the main EC phase for electronic transport. However, the latter phase NSFO also assists the oxygen ionic transport. The basic idea for choosing this system is as follows: (i) the Fe-based perovskite oxides (*e.g.* Fe-doped Ln (Ln = La series elements) SrO_3) are reported to show a higher stability than Co/Ni-based oxides under a reducing or CO_2 atmosphere[26] and show good p-type electronic conductivity;[27,28] (ii) in a recent study, covering a large number of 10 atm% rare earth doped cerias, synthesized under similar conditions, Nd-doping ceria is reported to exhibit the highest ionic conductivity.[29] (iii) Based on the common ion effects, which was defined as the suppression of dissociation of a weak electrolyte containing a common ion, we chose the same element (Nd) in both OIC and EC phases in order to reduce the element diffusion between the two phases;[30] (iv) the concentration of the highly EC component NSFO in the dual phase materials was chosen to be 40 wt% in order to guarantee a continuous electron transport in a percolation network.

Therefore, the aim of this study is the development of a 40NSFO–60CNO dual phase membrane *via* a facile one-pot EDTA–citric acid sol–gel method. The phase structure and stability as well as oxygen permeation have been investigated under different atmospheres (especially CO_2 and CH_4) at high temperatures.

Experimental

Preparation of powders and membranes

The 40 wt% $Nd_{0.6}Sr_{0.4}FeO_{3-\delta}$–60 wt% $Ce_{0.9}Nd_{0.1}O_{2-\delta}$ (40NSFO–60CNO) dual phase powder mixture was synthesized *via* a facile *in situ* one-pot EDTA–citric acid sol–gel method. The appropriate stoichiometric metal nitrates $Sr(NO_3)_2$, $Fe(NO_3)_3$, $Ce(NO_3)_3$ and $Nd(NO_3)_3$ in aqueous solutions were mixed in a beaker. After stirring for 20 min, the calculated amounts of citrate and EDTA were added and the pH value was adjusted to ~9 by ammonia. The molar ratio of citric acid : EDTA : total metal ions was 1.5 : 1 : 1. Then the solutions were stirred while heated to 150 °C, until the water evaporated and a gel was formed. The gels were calcined in air at 600 °C in a furnace to remove the organic compounds by combustion, and the primary powders were obtained. The resulting powders were calcined at 950 °C for 10 h in air. The 40NSFO–60CNO powders were pressed to disk membranes under a pressure of 5 MPa in a stainless steel module with a diameter of 18 mm to get green disk membranes. These green disks were pressure-less sintered at 1400 °C in air for 5 h in air. The surfaces of the disks were carefully polished to 0.60 mm thickness by using 1200 grit-sand paper (average particle diameter 15.3 μm), then the membranes were washed with ethanol.

Characterization of membranes

The phase structure of the dual phase membranes after sintering at 1400 °C for 5 h in air was determined by X-ray diffraction (XRD, using a D8 Advance, Bruker-AXS, with Cu Kα radiation, $\lambda = 1.5418$ Å). Data sets were recorded at room temperature in a step-scan mode in the 2θ range of 20–80° with intervals of 0.02°. *In situ* XRD was conducted in a high-temperature cell HTK-1200N (Anton-Paar) from 30 °C to 1000 °C. The *in situ* XRD tests in air and a 50 vol% CO_2/50 vol% N_2 atmosphere were performed with a heating rate of 12 °C min^{-1}. At each temperature step, the sample was held for 50 minutes for thermal equilibrium before diffraction data collection. The disc membranes were studied by scanning electron microscopy (SEM) using a JEOL JSM-6700F at an excitation voltage of 20 keV. The element distribution in the grains of the fresh dual phase membranes under study was investigated on the same electron microscope by energy dispersive X-ray spectroscopy (EDXS), Oxford Instruments INCA-300 EDX spectrometer with an ultra-thin window at an excitation voltage of 20 keV.

Oxygen permeation performances of membranes

The oxygen permeation was studied in a home-made high-temperature oxygen permeation permeator, which is described in a previous paper.[31] The disc membranes were sealed onto a quartz tube at 950 °C for 5 hours with a gold paste (Heraeus, Germany), the side wall of the membrane disc was also covered with gold paste to avoid any radial contribution to the oxygen permeation flux. The effective areas of the membranes for oxygen permeation were 0.785 cm^2. Air as feed gas was fed into one side of the membrane and He or CO_2 as sweep gases were fed into the other side of the membrane. All the inlet gas flow rates were controlled by gas mass flow controllers (Bronkhorst, Germany) and all flow rates were regularly calibrated by using a bubble flow meter. Synthetic air (20% O_2 and 80% N_2) with a flow rate of 150 cm^3 min^{-1} was the feed; a mixture of He or CO_2 (49 cm^3 min^{-1}) and Ne (1 cm^3 min^{-1}) as the internal standard gas was fed to the sweep side. An Agilent 6890A gas chromatograph with a Carboxen 1000 column was employed to analyze the gas mixture. All disks were carefully polished with 1200 mesh sandpaper from both sides to achieve a 0.6 mm membrane thickness. Before oxygen permeation, both surfaces of the polished disks were cleaned with ethanol. To improve the oxygen surface exchange rate on the air side, the 40NSFO–60CNO membrane was coated with a $La_{0.6}Sr_{0.4}CoO_{3-\delta}$ (LSC) porous layer, which shows a good oxygen reducing activity when it acts as the cathode material for SOFC.[32] After coating with the LSC layer, the membrane was calcined at 950 °C for 2 h.

In addition, the 40NSFO–60CNO dual phase membrane has been used as a membrane reactor for POM. The membrane reactor configuration for POM was described elsewhere.[33] A Ni-based catalyst (0.3 g, Süd Chemie AG) was loaded on top of the membrane disc and then the temperature of the reactor was increased to 950 °C with a heating rate of 2 °C min^{-1}. All gas lines to the reactor and the gas chromatograph were heated to 180 °C. High-purity methane with He dilution was used as the reactant for the POM to synthesis gas. Gas composition was analyzed by an online gas chromatograph (GC, Agilent 6890A).

Results and discussion

Characterization of the 40NSFO–60CNO dual phase material

The XRD patterns of the as-obtained NSFO, CNO, 40NSFO–60CNO powders calcined at 950 °C for 10 h in air and of the 40NSFO–60CNO dual phase membrane sintered at 1400 °C for 5 h in air are shown in Fig. 1c. From the XRD patterns, it can be concluded that both the calcined dual phase powder and the sintered membranes are composed of only the cubic fluorite CNO phase (see Fig. 1a, space group 225, *Fm*3*m*) and the orthorhombic distorted perovskite NSFO (see Fig. 1b, space group 74, *Imma*). Table S1† summarizes the lattice parameters of NSFO and CNO as pure phases, in the 40NSFO–60CNO dual phase powder, and in the 40NSFO–60CNO dual phase membrane. It was found that the lattice parameters of the pure CNO and NSFO phases are similar in the 40NSFO–60CNO dual phase powder and in the sintered membrane. The lattice volume of CNO in the 40NSFO–60CNO composite powders is also similar to the single CNO powder. There are no additional phases (such as $NdFeO_3$ and $NdSrFeO_4$) even though the dual phase mixture was prepared by a facile one-pot EDTA–citric acid sol–gel method, which indicate good chemical compatibility between the two phases NSFO and CNO. Fig. 2 presents SEM, BSEM and EDXS pictures of the as-prepared 40NSFO–60CNO dual phase membrane after sintering at 1400 °C for 5 h in air at two different magnifications before polishing. SEM images (Fig. 2a and b) reveal that the micro-sized grains are packed closely. The CNO and NSFO grains are distributed very uniformly in the membrane; no major cracks are visible. In the bulk only a few non-connected pores were observed. The NSFO and CNO grains could be distinguished by BSEM and EDXS (Fig. 2c–f). The dark grains in BSEM are NSFO and the light ones are CNO, since the contribution of the backscattered electrons to the SEM signal intensity is proportional to the atomic number. The same information is provided by EDXS (Fig. 2e and f), which suggests that the green color (dark in the black-and-white version) is an overlap of the Nd, Fe and Sr signals, whereas the yellow color (light) stems from an average of the Ce and Nd signals. The average grain size areas of NSFO and CNO have been estimated to be 0.157 μm^2 and 0.210 μm^2 from the analysis of 130 grains, respectively. The STEM and EDXS mappings shown in Fig. S1† indicate that the membrane consists of a micro-scale mixture of well-separated NSFO (mixed ion-electron conductor) and CNO (oxygen ions conductor) grains forming a percolation network.

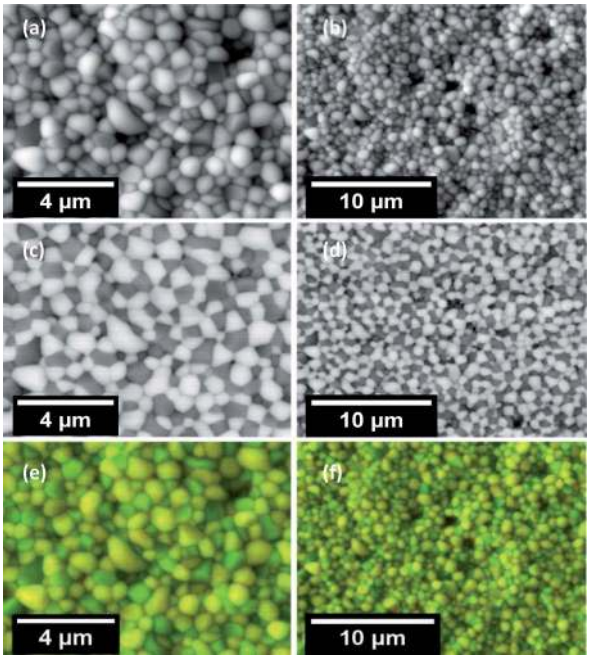

Fig. 2 SEM (a and b), BSEM (c and d), and EDXS (e and f) images of the 40NSFO–60CNO membrane after sintering at 1400 °C for 5 h in air before polishing (see Fig. 1). For the EDXS mapping in Fig. 3e and f, superimpositions of the Nd Lα, Sr Kα and Fe Kα (green) and Nd Lα and Ce Lα (yellow) have been used.

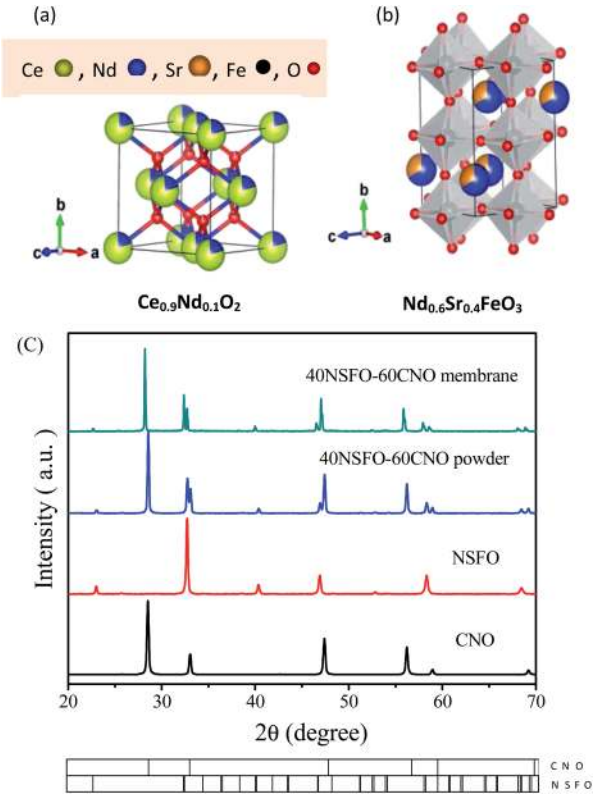

Fig. 1 (a) Structure of (a) cubic fluorite $Ce_{0.9}Nd_{0.1}O_2$ (CNO), and (b) orthorhombic distorted perovskite $Nd_{0.6}Sr_{0.4}FeO_3$ (NSFO); (c) XRD patterns of CNO, NSFO and the dual phase 40NSFO–60CNO powder calcined at 950 °C for 10 h and the 40NSFO–60CNO dual phase membrane sintered at 1400 °C for 5 h.

Phase stability of the 40NSFO–60CNO dual phase material

Fig. 3a shows the *in situ* XRD patterns of the sintered 40NSFO–60CNO dual phase membrane after being crushed into powder, collected in air with increasing temperature from 30 °C to 1000 °C. During heating, no additional reflexes except those of NSFO and CNO phases were observed, suggesting that the phases of CNO and NSFO remain unchanged in the 40NSFO–60CNO dual phase material. Additionally, the

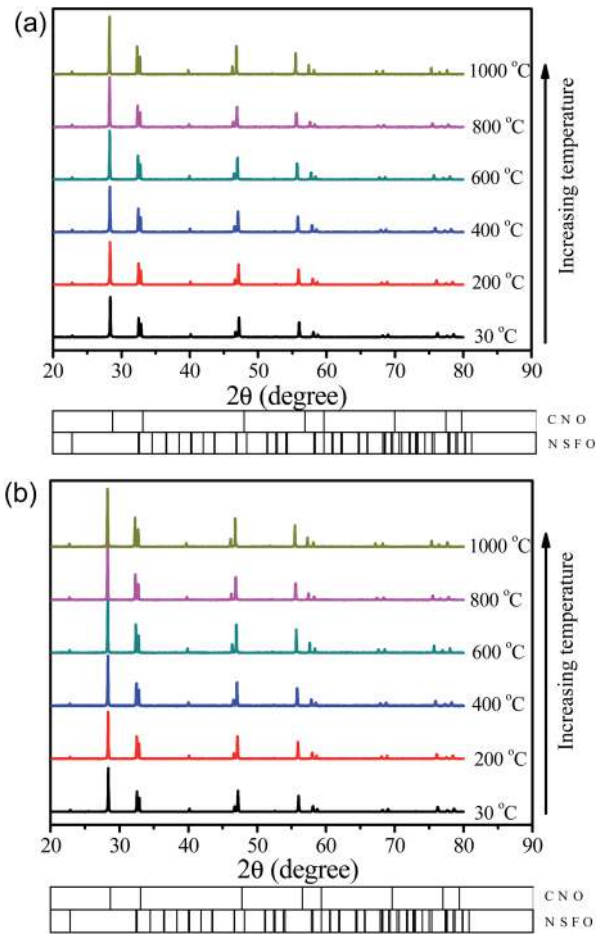

Fig. 3 *In situ* XRD patterns of the 40NSFO–60CNO dual phase membrane sintered at 1400 °C for 5 h after being crushed for increasing temperature in (a) air and (b) in 50 vol% CO_2 and 50 vol% N_2. *Conditions*: heating rate = 12 °C min^{-1}; equilibration time at each temperature: 50 min for recording the XRD data at each temperature; *F* total = 100 cm^3 min^{-1}.

high-temperature phase stability in a CO_2 containing atmosphere has been studied by *in situ* XRD (Fig. 3b) between 30 °C and 1000 °C in an atmosphere of 50 vol% CO_2 and 50 vol% N_2. As can be seen from Fig. 3b, the dual phase membrane completely keeps its two phases of NSFO and CNO. CO_2 is known to be a sensitive gas to most of the single phase perovskite OTM materials which especially contain a high basicity element such as Ba. On the other hand, it has been reported that a phase transition occurs at moderate and high temperatures in the Co-containing single phase perovskite OTM materials, also for some dual phase membranes.[26,34] However, no carbonate formation or phase transition could be observed in our dual phase membrane 40NSFO–60CNO in an atmosphere of 50 vol% CO_2 and 50 vol% N_2 in the temperature range of 30 °C and 1000 °C suggesting that the dual phase membrane 40NSFO–60CNO is thermally and chemically stable both in air and in CO_2 up to 1000 °C. The long-time stability of the oxygen flux with pure CO_2 as the sweep gas also confirmed the stability of our dual-phase membrane in CO_2 (Fig. 6).

Oxygen permeation and chemical stability under CO_2

Fig. 4 shows the oxygen permeation flux through the 40NSFO–60CNO dual phase membrane as a function of temperature with pure He and CO_2 as sweep gases with/without $La_{0.6}Sr_{0.4}CoO_{3-\delta}$ (LSC) porous layer coating of the 40NSFO–60CNO. All data were collected after the oxygen permeation had reached a steady state (after about 20 h.). The reason for this experimental finding maybe because it is related to the oxygen exchange reactions on the gas–solid interface of the membranes. The gas–solid interface exchange is slow because of the dense and small membrane surface area. On the other hand, the steady time is related to the dual phase material or composition ratio. This behaviour has been reported in many dual phase membranes, such as *x* wt% $Fe_2O_{3-\delta}$–(100 − *x*) wt% $Ce_{0.9}Gd_{0.1}O_{2-\delta}$ (*x* = 25, 40, 50),[21] 40 wt% $Pr_{0.6}Sr_{0.4}Co_{0.5}Fe_{0.5}O_{3-\delta}$–60 wt% $Ce_{0.9}Pr_{0.1}O_{2-\delta}$,[34] 25 wt% $Sm_{0.6}Sr_{0.4}FeO_{3-\delta}$–75 wt% $Ce_{0.85}Sm_{0.15}O_{1.925}$.[35] As shown in Fig. 4a, the oxygen permeation fluxes through all of our dual phase membranes increase with increasing temperature. For the dual phase membrane without LSC coating, oxygen permeation fluxes of 0.26 and 0.21 cm^3 min^{-1} cm^{-2} are found at 950 °C for the pure sweep gases He and CO_2. On the other hand, it was found that when the temperature increases from 850 °C

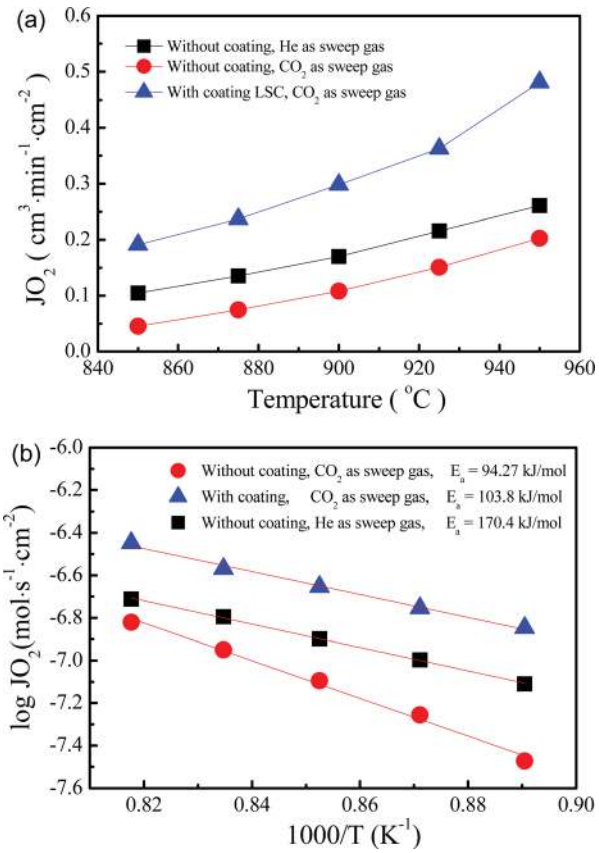

Fig. 4 Oxygen permeation flux through the 40NSFO–60CNO dual phase membrane as a function of temperature with pure He/CO_2 as the sweep gas for membranes without and with porous $La_{0.6}Sr_{0.4}CoO_{3-\delta}$ (LSC) coating on the air side. *Conditions*: 150 cm^3 min^{-1} air as feed gas, 49 cm^3 min^{-1} He/CO_2 as sweep gas; 1 cm^3 min^{-1} Ne as internal standard gas. Membrane thickness: 0.6 mm.

to 950 °C, the oxygen permeation flux through the membrane with an LSC porous layer coating on the air side increases from 0.21 $cm^3\ min^{-1}\ cm^{-2}$ to a stable value of 0.48 $cm^3\ min^{-1}\ cm^{-2}$ for a membrane thickness of 0.6 mm, when CO_2 has been used as a sweep gas. The 40CNO–60NSFO dual phase membrane shows lower oxygen permeation flux than most of the single perovskite membranes for He as a sweep gas in comparison with literature data (Table 1). However, when using CO_2 as a sweep gas, the oxygen permeation flux is much higher than reported for the single phase and other dual phase oxygen permeable membranes and even higher than those of some Co-containing dual phase membranes.[36]

Furthermore, the Arrhenius plot (Fig. 4b) indicates that oxygen permeation can be described by a single apparent activation energy in the temperature range of 850–950 °C with pure CO_2 as the sweep gas. It has been suggested that the change of activation energy is caused by the change in rate-controlling process.[22,37,38] Here, the fluorite phase is the main phase in the dual-phase system. And the oxygen permeation flux for the LSC coated 40CNO–60NSFO dual phase membrane is two times higher than that of the uncoated coating membrane (see Fig. 6). The rate-limiting step of oxygen permeation through 40CNO–60NSFO maybe related to oxygen surface exchange. However, determination of the limiting transport in the 40CNO–60NSFO dual phase membrane was not performed. Further investigations will be carried out in the future. Meanwhile, it is accepted that single activation energy is an important indication that there is no phase transformation in the membrane under study.[39] This conclusion is in agreement with the finding that the oxygen flux with pure CO_2 as a sweep gas is found to be long-time stable (see Fig. 6).

Fig. 5 shows the reversibility of the oxygen permeation flux through the 40NSFO–60CNO membrane without LSC coating when periodically changing the sweep gas between He and CO_2 at 1000 °C. When using He as a sweep gas, a stable oxygen permeation flux of 0.26 $cm^3\ min^{-1}\ cm^{-2}$ can be obtained,

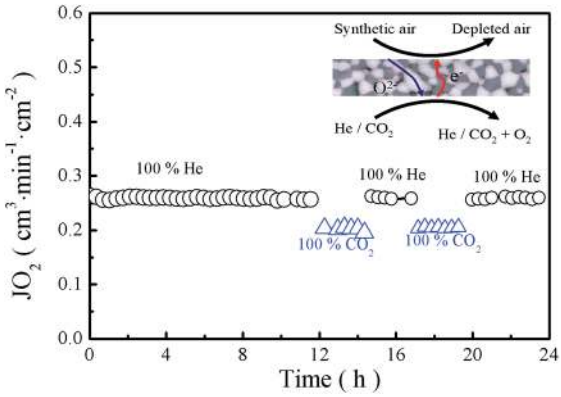

Fig. 5 Oxygen permeation fluxes as a function of time while periodically changing the sweep gas. *Conditions*: 150 $cm^3\ min^{-1}$ air as feed gas, 49 $cm^3\ min^{-1}$ He and 1 $cm^3\ min^{-1}$ Ne or 49 $cm^3\ min^{-1}$ CO_2 and $cm^3\ min^{-1}$ Ne as sweep gas; membrane thickness: 0.6 mm. Temperature: 950 °C. Without LSC coating.

whereas the oxygen permeation flux decreases immediately to the slightly lower value of 0.21 $cm^3\ min^{-1}\ cm^{-2}$, if CO_2 instead of He is used as the sweep gas. This behavior was also observed in the previous studies of a CO_2-stable dual phase membrane which is ascribed to the slight inhibiting effect of CO_2 on the oxygen surface-exchange. This behaviour is different from previous findings on the perovskite-type membranes containing high basicity alkaline-earth metals (such as Ba) *e.g.* $Ba_{0.5}Sr_{0.5}Co_{0.8}Fe_{0.2}O_{3-\delta}$ (BSCF),[17] $BaCo_xFe_yZr_zO_{3-\delta}$(BCFZ),[18] and $Ba(Co_{0.4}Fe_{0.4}Nb_{0.2})O_{3-\delta}$,[19] where the oxygen permeation flux decreases sharply due to the formation of carbonates if CO_2 was present. But the chemical stability of the perovskite-type membrane material strongly depends on the A and/or B-site composition as well. Thus, the primary approach used to improve the CO_2 stability of the perovskite-type materials is to modify the composition by doping other metals into the

Table 1 Steady-state oxygen permeation flux (J_{O_2}) through different OTM membranes in disk geometries

Membrane materials	Thickness (mm)	Temperature (°C)	Oxygen flux ($cm^3\ min^{-1}\ cm^{-2}$) air/He	Oxygen flux ($cm^3\ min^{-1}\ cm^{-2}$) air/CO_2	Ref.
$Ba_{0.5}Sr_{0.5}Co_{0.8}Fe_{0.2}O_{3-\delta}$ [a]	1	875	1.9	0	16
$La_{0.6}Sr_{0.4}Co_{0.8}Fe_{0.2}O_{3-\delta}$ [a]	1	900	—	0.1	26
$La_{0.9}Sr_{0.1}FeO_{3-\delta}$ [a]	1	1000	0.22	—	25
40 wt% $NiFe_2O_4$–60 wt% $Ce_{0.9}Gd_{0.1}O_{2-\delta}$ [a]	0.5	950	0.18	0.16	7 and 20
40 wt% Fe_2O_3–60 wt% $Ce_{0.9}Gd_{0.1}O_{2-\delta}$ [a]	0.5	950	0.10	0.08	21
40 wt% $Mn_{1.5}Co_{1.5}O_{4-\delta}$–60 wt% $Ce_{0.9}Pr_{0.1}O_{2-\delta}$ [a]	0.5	1000	0.22	0.20	22
40 wt% $Pr_{0.6}Sr_{0.4}FeO_{3-\delta}$–60 wt% $Ce_{0.9}Pr_{0.1}O_{2-\delta}$ [a]	0.6	950	0.27	0.18	8
25 wt% $Sm_{0.6}Ca_{0.4}CoO_{3-\delta}$–75 wt% $Ce_{0.8}Sm_{0.2}O_{2-\delta}$ [b]	0.5	950	0.23	0.16	36
40 wt% $Nd_{0.6}Sr_{0.4}FeO_{3-\delta}$–60 wt% $Ce_{0.9}Nd_{0.1}O_{2-\delta}$ [a]	0.6	950	0.26	0.21	This work
40 wt% $Nd_{0.6}Sr_{0.4}FeO_{3-\delta}$–60 wt% $Ce_{0.9}Nd_{0.1}O_{2-\delta}$ [c]	0.6	950	—	0.48	This work

[a] Both sides of the membrane uncoated with $La_{0.6}Sr_{0.4}CoO_{3-\delta}$ porous layer. [b] Both sides of the membrane coated with 25 wt% $Sm_{0.6}Ca_{0.4}CoO_{3-\delta}$–75 wt% $Ce_{0.8}Sm_{0.2}O_{2-\delta}$ porous layer. [c] Air side of the membrane coated with $La_{0.6}Sr_{0.4}CoO_{3-\delta}$ porous layer.

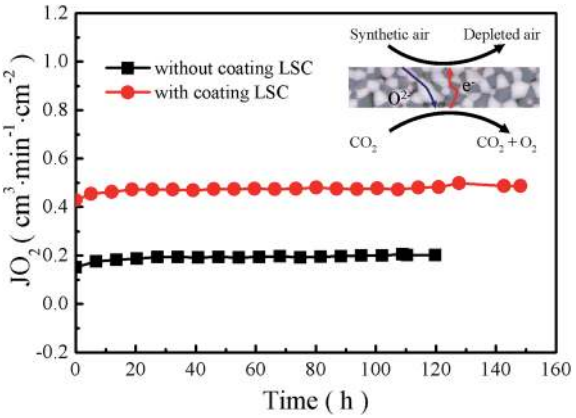

Fig. 6 Oxygen permeation flux through the 40NSFO–60CNO dual phase membrane as a function of time with pure CO_2 as the sweep gas for membranes without and with porous LSC coating. *Conditions*: 150 cm^3 min^{-1} air as feed gas, 49 cm^3 min^{-1} CO_2 as sweep gas; 1 cm^3 min^{-1} Ne as internal standard gas. Membrane thickness: 0.6 mm. Temperature: 950 °C.

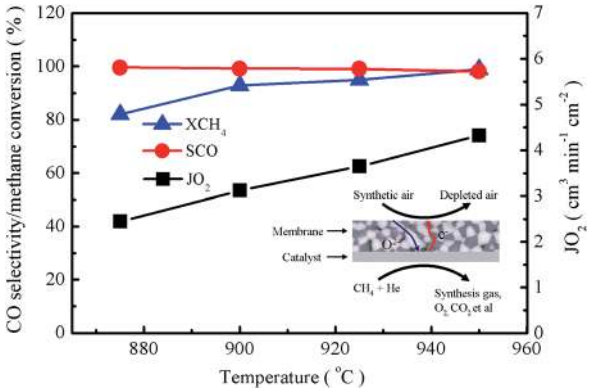

Fig. 7 Influence of temperature on CH_4 conversion (▲), CO selectivity (●) and oxygen permeation flux (■) through the 40NSFO–60CNO dual phase membrane without LSC coating on the air side in the POM to synthesis gas. *Conditions*: 150 cm^3 min^{-1} air as feed gas, 11 cm^3 min^{-1} He with 8.27 cm^3 min^{-1} CH_4 as sweep gas; 1 cm^3 min^{-1} Ne as internal standard gas. Membrane thickness: 0.6 mm.

perovskite structure. It has been reported that CO_2-tolerant materials (such as $La_{0.6}Sr_{0.4}Co_{0.8}Fe_{0.2}O_{3-\delta}$,[26,40,41] $La_{0.6}Ca_{0.4}Co_{0.8}Fe_{0.2}O_{3-\delta}$)[42] can be obtained by doping a less basic alkaline-earth metal or non-alkaline earth metals (such as La, Ca).[40–43] In our study the 40NSFO–60CNO membrane has good reversibility of the oxygen permeation fluxes and good chemical stability in a CO_2 atmosphere.

The time dependence of the oxygen permeation flux through the 40NSFO–60CNO dual phase composite membrane with and without an LSC coating for CO_2 as the sweep gas is shown in Fig. 6 During the whole oxygen permeation, oxygen permeation fluxes for the uncoated and coated membranes are about 0.21 cm^3 cm^{-2} min^{-1} and 0.48 cm^3 cm^{-2} min^{-1} respectively at 1000 °C and no decrease with time was found. Combining the *in situ* XRD, the reversibility of the oxygen permeation measurements when switching the sweep gases from CO_2 to He, and the stable oxygen permeation fluxes on our 40NSFO–60CNO, we can exclude chemical reactions between the two NSFO and CNO phases involved such as those reported in previous studies of dual phase membranes.[7,8,20,21]

40NSFO–60CNO membrane reactor in the partial oxidation of methane (POM) to synthesis gas

Fig. 7 presents the temperature influence on CH_4 conversion, CO selectivity and oxygen permeation flux through the 40NSFO–60CNO dual phase membrane in the POM to synthesis gas. It was observed that the oxygen permeation fluxes increased from 2.44 cm^3 min^{-1} cm^{-2} to 4.33 cm^3 min^{-1} cm^{-2} and methane conversion increased from 82.1% to 98.8% with increasing temperatures from 875 °C to 950 °C while the CO selectivity slightly decreased from 99.6% to 98.1%. This behavior is in good agreement with the observation in previous studies.[8,33] The reasons for this behavior are explained as follows: (1) the increased oxygen permeation flux was due to the increase of the oxygen diffusion rate through the 40NSFO–60CNO membrane and the faster surface kinetics with increasing temperature. (2) Further, the increasing amount of permeated oxygen leads to the increase of the methane conversion. (3) The decrease of the CO selectivity with increasing temperature is ascribed to some excess oxygen in comparison to the amount of oxygen required for the stoichiometry of POM.

Fig. 8 shows the influence of the methane concentration in the feed on CH_4 conversion, CO selectivity and oxygen permeation flux through the 40NSFO–60CNO dual phase membrane in the POM to synthesis gas at 950 °C. As shown in Fig. 8, with increasing methane concentration, the methane conversion decreases from 99.9% to 92.1% while the CO selectivity increases from 97.4% to 99.6% and the oxygen permeation fluxes increase from 3.16 cm^3 min^{-1} cm^{-2} to 5.06 cm^3 min^{-1} cm^{-2} when the methane concentrations of the feed increase from 30% to 60%. This experimental finding can be explained as follows: (1) the

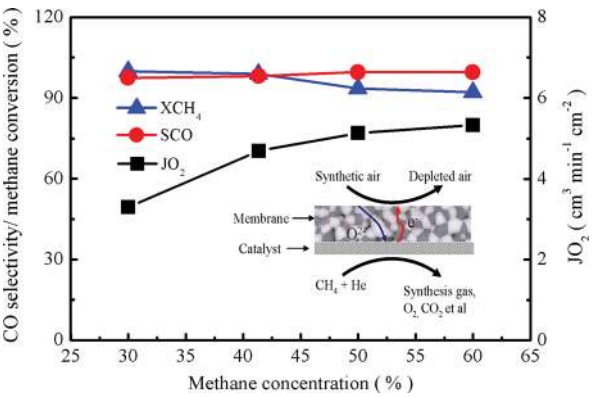

Fig. 8 Influence of methane concentration on CH_4 conversion (▲), CO selectivity (●) and oxygen permeation flux (■) through the 40NSFO–60CNO dual phase membrane without an LSC coating on the air side in the POM to synthesis gas. *Conditions*: feed side: fair = 150 cm^3 min^{-1}, sweep side: $F_{He} + F_{CH_4} + F_{Ne} = 20$ cm^3 min^{-1}, 1 cm^3 min^{-1} Ne as internal standard gas, membrane thickness: 0.6 mm. Temperature: 950 °C.

increased oxygen permeation flux was due to the increased driving force for oxygen permeation with increasing methane concentration. (2) However, at high methane concentrations the oxygen flux is increased, but more methane is available than that needed for the stoichiometric POM. Thus, the methane conversion is reduced. (3) The higher the methane concentration, the lesser CO is oxidized to CO_2 which results in a higher CO selectivity.

Conclusions

In this work, a novel dual phase oxygen transporting membrane with the composition 40 wt% $Nd_{0.6}Sr_{0.4}FeO_{3-\delta}$–60 wt%$Ce_{0.9}Nd_{0.1}O_{2-\delta}$ (40NSFO–60CNO) has been developed by using the *in situ* EDTA–citric acid sol–gel synthesis method. A stable oxygen flux of 0.48 $cm^3\ min^{-1}\ cm^{-2}$ can be achieved at 950 °C when using CO_2 as the sweep gas for a 0.6 mm thick membrane with a porous $La_{0.6}Sr_{0.4}CoO_{3-\delta}$ (LSC) coating on the air side. The 40NSFO–60CNO membrane was stable for more than 150 h when using pure CO_2 as the sweep gas. The 40NSFO–60CNO dual phase reactor was successfully used for the POM to syngas. Methane conversion was found to be higher than 99.0% with 98.0% CO selectivity, a 4.33 $cm^3\ min^{-1}\ cm^{-2}$ oxygen permeation flux was obtained under steady state conditions at 950 °C. The results demonstrate that our 40NSFO–60CNO dual phase membrane is not only stable in CO_2 but also in reducing atmospheres, which makes it a promising membrane material for the oxyfuel process for CO_2 capture. However, the oxygen permeation flux is lower than that for the industrial application requirement (1 $cm^3\ min^{-1}\ cm^{-2}$).[43] In future, further research is needed to improve the oxygen flux of this dual phase membrane by doping as well by technical measures such as asymmetric membrane structures[12,44,45] or by surface enlargement as demonstrated for a hollow fibre structure.[46]

Acknowledgements

The authors acknowledge financial support from the Sino-German Centre for Science Promotion (GZ 676, GZ911). H. H. Wang greatly acknowledges the financial support by National Science Fund for Distinguished Young Scholars of China (no. 21225625). The authors also greatly acknowledge F. Steinbach for technical support and Prof H. Jiang for useful discussions.

References

1 Z. P. Shao, S. M. Haile, J. Ahn, P. D. Ronney, Z. L. Zhan and S. A Barnett, *Nature*, 2005, **435**, 795.
2 Z. P. Shao and S. M. Haile, *Nature*, 2004, **431**, 170.
3 H. Q. Jiang, H. H. Wang, F. Y. Liang, S. Werth, T. Schiestel and J. Caro, *Angew. Chem., Int. Ed.*, 2009, **48**, 2983.
4 H. Q. Jiang, Z. W. Cao, S. Schirrmeister, T. Schiestel and J. Caro, *Angew. Chem., Int. Ed.*, 2010, **49**, 5656.
5 Z. W. Cao, H. Q. Jiang, H. X. Luo, S. Baumann, W. A. Meulenberg, J. Assmann, L. Mlecko, Y. Liu and J. Caro, *Angew. Chem., Int. Ed.*, 2013, **52**, 13794.
6 X. Y. Tan, L. L. Shi, G. Z. Hao, B. Meng and S. M. Liu, *Sep. Purif. Technol.*, 2012, **96**, 89.
7 H. X. Luo, K. Efimov, H. Q. Jiang, A. Feldhoff, H. H. Wang and J. Caro, *Angew. Chem., Int. Ed.*, 2011, **50**, 759.
8 H. X. Luo, H. Q. Jiang, T. Klande, Z. H. Cao, F. Y. Liang, H. H. Wang and J. Caro, *Chem. Mater.*, 2012, **24**, 2148.
9 S. M. Hashim, A. R. Mohamed and S. Bhatia, *Adv. Colloid Interface Sci.*, 2010, **160**, 88.
10 V. M. Goldschmidt, *Die Naturwissenschaften*, 1926, **21**, 477.
11 J. F. Vente, W. G. Haije and Z. S. Rak, *J. Membr. Sci.*, 2006, **276**, 178.
12 S. Baumann, J. M. Serra, M. P. Lobera, S. Escolástico, F. Schulze-Küppers and W. A. Meulenberg, *J. Membr. Sci.*, 2011, **377**, 198.
13 H. Kruidhof, H. J. M. Bouwmeester, R. H. E. v. Doorn and A. J. Burggraaf, *Solid State Ionics*, 1993, **63–65**, 816.
14 K. Efimov, Q. Xu and A. Feldhoff, *Chem. Mater.*, 2010, **22**, 5866.
15 J. Kniep and Y. S. Lin, *Ind. Eng. Chem. Res.*, 2011, **50**, 7941.
16 M. Arnold, T. M. Gesing, J. Martynczuk and A. Feldhoff, *Chem. Mater.*, 2008, **20**, 5851.
17 M. Arnold, H. H. Wang and A. Feldhoff, *J. Membr. Sci.*, 2007, **293**, 44.
18 O. Czuprat, M. Arnold, S. Schirrmeister, T. Schiestel and J. Caro, *J. Membr. Sci.*, 2010, **364**, 132.
19 J. X. Yi, M. Schroeder, T. Weirich and J. Mayer, *Chem. Mater.*, 2010, **22**, 6246.
20 H. X. Luo, H. Q. Jiang, K. Efimov, H. H. Wang and J. Caro, *AIChE. J.*, 2011, **57**, 2738.
21 H. X. Luo, H. Q. Jiang, K. Efimov, F. Y. Liang, H. H. Wang and J. Caro, *Ind. Eng. Chem. Res.*, 2011, **50**, 13508.
22 H. X. Luo, H. Q. Jiang, T. Klande, F. Y. Liang, Z. W. Cao, H. H. Wang and J. Caro, *J. Membr. Sci.*, 2012, **423–424**, 450.
23 X. F. Zhu, H. Y. Liu, Y. Cong and W. S. Yang, *Chem. Commun.*, 2012, **48**, 251.
24 J. Xue, Q. Liao, Y. Y. Wei, Z. Li and H. H. Wang, *J. Membr. Sci.*, 2013, **443**, 124.
25 Z. T. Wang, W. P. Sun, Z. W. Zhu, T. Liu and W. Liu, *ACS Appl. Mater. Interfaces*, 2013, **5**, 11038.
26 T. Klande, O. Ravkina and A. Feldhoff, *J. Membr. Sci.*, 2013, **437**, 122.
27 A. A. Yaremchenko, V. V. Kharton, A. P. Viskup, E. N. Naumovich, V. N. Tikhonovich and N. M. Lapchuk, *Solid State Ionics*, 1999, **120**, 65.
28 V. V. Kharton, A. V. Kovalevsky, M. V. Patrakeev, E. V. Tsipis, A. P. Viskup, V. A. Kolotygin, A. A. Yaremchenko, A. L. Shaula, E. A. Kiselev and J. o. C. Waerenborgh, *Chem. Mater.*, 2008, **20**, 6457.
29 S. Omar, E. D. Wachsman, J. L. Jones and J. C. Nino, *J. Am. Ceram. Soc.*, 2009, **92**, 2674.
30 http://www.en.wikipedia.org/wiki/Common-ion_effect.
31 H. X. Luo, B. B. Tian, Y. Y. Wei, H. H. Wang, H. Q. Jiang and J. Caro, *AIChE J.*, 2010, **56**, 604.
32 Y. K. Tao, J. Shao, W. G. Wang and J. X. Wang, *Fuel Cells*, 2009, **5**, 679.
33 H. X. Luo, Y. Y. Wei, H. Q. Jiang, W. H. Yuan, Y. X. Lv, J. Caro and H. H. Wang, *J. Membr. Sci.*, 2010, **350**, 154.
34 F. Y. Liang, H. X. Luo, K. Partovi, O. Ravkina, Z. W. Cao, Y. Liu and J. Caro, *Chem. Commun.*, 2014, **50**, 2451.

35 X. F. Zhu, H. Y. Liu, Q. M. Li, Y. Cong and W. S. Cong, *Solid State Ionics*, 2011, **185**, 27.
36 H. B. Li, Y. Liu, X. F. Zhu, Y. Cong, S. P. Xu, W. Q. Xu and W. S. Yang, *Sep. Purif. Technol.*, 2013, **114**, 31.
37 S. W. Leea, K. S. Leeb, S. K. Woob, J. W. Kim, T. Ishiharad and D. K. Kim, *Solid State Ionics*, 2003, **158**, 287.
38 J. Sunarso, S. Baumann, J. M. Serra, W. A. Meulenberg, S. Liu, Y. S. Lin and J. C. Diniz da Costa, *J. Membr. Sci.*, 2011, **377**, 198.
39 J. H. Tong, W. S. Yang, B. C. Zhu and R. Cai, *J. Membr. Sci.*, 2002, **203**, 175.
40 J. M. Serra, J. G. Fayos, S. Baumann, F. S. Küppers and W. A. Meulenberg, *J. Membr. Sci.*, 2013, **447**, 297.
41 X. Y. Tan, N. Liu, B. Meng, J. Sunarso, K. Zhang and S. M. Liu, *J. Membr. Sci.*, 2012, **389**, 216.
42 K. Efimov, T. Klande, N. Judizki and A. Feldhoff, *J. Membr. Sci.*, 2012, **389**, 205.
43 B. C. H. Steele, *Curr. Opin. Solid State Mater. Sci.*, 1996, **1**, 684.
44 M. P. Lobera, J. M. nt, S. P. Foghmoes, M. Søgaard and A. Kaiser, *J. Membr. Sci.*, 2011, **385–386**, 154.
45 A. Kaiser, S. Foghmoes, C. Chatzichristodoulou, M. Søgaard, J. A. Glasscock, H. L. Frandsen and P. V. Hendriksen, *J. Membr. Sci.*, 2011, **378**, 51.
46 X. Y. Tan, Z. G. Wang, B. Meng, X. X. Meng and K. Li, *J. Membr. Sci.*, 2010, **352**, 189.